Detection of an X-ray jet in 3C 371 with *Chandra*

Joseph E. Pesce
George Mason University, Dept. of Physics & Astronomy, 4400 University Dr., M/S 3F3, Fairfax, VA, 22030-4444, and
Eureka Scientific, Inc.

Rita M. Sambruna
George Mason University, Dept. of Physics & Astronomy and School of Computational Sciences, 4400 University Dr., M/S 3F3, Fairfax, VA, 22030-4444

F. Tavecchio and L. Maraschi
Osservatorio Astronomico di Brera, via Brera 28, 20121 Milano, Italy

C. C. Cheung
Physics Department, MS 057, Brandeis University, Waltham, MA 02454

C. Megan Urry
STScI, 3700 San Martin Dr., Baltimore, MD 21218

R. Scarpa
European Southern Observatory, 3107 Slonso de Cordova, Santiago, Chile

ABSTRACT

We report the detection at X-rays of the radio/optical jet of 3C 371, from a short (10 ks) *Chandra* exposure in March 2000. We also present a new *MERLIN* observation at 1.4 GHz together with a renalysis of the archival *HST* WFPC2 F555W image. Despite the limited signal-to-noise ratio of the *Chandra* data, the X-ray morphology is clearly different from that of the radio/optical emission, with the brightest X-ray knot at 1.7″ from the nucleus and little X-ray emission from the brightest radio/optical knot at 3.1″. We construct the spectral energy distributions for the two emission regions at 1.7″ and 3.1″. Both show that the X-ray flux is below the extrapolation from the radio-to-optical continuum, suggesting moderately beamed synchrotron from an electron population with decreasing high energy cut-off as a plausible emission mechanism.

Subject headings: galaxies: active — galaxies: jets — (galaxies:) quasars: individual (3C 371) — X-rays: galaxies

1. Introduction

Jets are relatively common in extragalactic radio sources (e.g., Bridle & Perley 1984), and undoubtedly represent a trace of the energy transport from the nucleus to the outer hot spots/radio lobes. Hence the interest of observations of jets at shorter wavelengths which can probe the sites of high energy particle acceleration and help determine their physical parameters. About a dozen

jets have been detected so far with *HST* [2] and ground-based telescopes (Sparks, Biretta, & Macchetto 1994). X-ray counterparts, however, were detected so far in only a handful of cases, including M87, 3C 273, and Cen A (Feigelson et al. 1981; Harris & Stern 1987; Biretta et al. 1991). This situation is rapidly changing now that the *Chandra* X-ray Observatory has enabled the discovery of new X-ray jets (e.g., Chartas et al. 2000; Wilson, Young, & Shopbell 2001), thanks to its excellent sensitivity in the 0.2–10 keV range and superb angular resolution (0.5″/pixel). Here we report the detection with *Chandra* of the X-ray counterpart of the radio-optical jet in the nearby radio source 3C 371 (z=0.051), which suggests that X-ray emission is indeed a common property of such jets.

3C 371 is classified as an intermediate source between BL Lacertae objects and radio galaxies (Miller 1975). Its radio morphology is characterized by two giant lobes and a 25″-long, one-sided jet (Wrobel & Lind 1990), typical of FRII galaxies. The jet-to-counterjet ratio from the radio is high, 1700:1, implying a viewing angle $\theta \lesssim 18^\circ$ and Lorentz factor $\Gamma \gtrsim 3.2$ (Gomez & Marscher 2000). However the lobe separation and intermediate classification suggest that 3C 371 is most likely seen at moderate viewing angles, near the upper limit quoted above.

The radio jet is well studied at milli-arcsecond resolution (Gomez & Marscher 2000 and references therein) and shows no superluminal motion, with an upper limit of $\sim 1.4h^{-1}c$. Optical emission from the jet was detected in ground-based (Nilsson et al. 1997) and in *HST* observations (Scarpa et al. 1999). The optical jet is 5″ long, with at least three knots from the nucleus; at 1.7″ (knot B, as in Scarpa et al. 1999), 3.1″ (knot A, the brightest), and 4.5″ (knot D, the faintest). Overall, the optical morphology tracks the radio one closely in the region of overlap (Scarpa et al. 1999).

As part of a *Chandra* AO1 program to image the extended X-ray environment of BL Lac objects in X-rays (Pesce et al. 2001, in prep.), we obtained a short (10 ks) exposure of 3C 371 with *Chandra*, resulting in a detection of the jet at X-rays. Here we present the *Chandra* observations, together with unpublished archival *MERLIN* 1.4 GHz data and a re-extraction of the fluxes from the *HST* F555W image (Scarpa et al 1999). Throughout this work we adopt $H_0 = 75$ km s^{-1} Mpc^{-1} and $q_0 = 0.5$, so at the distance of 3C 371 1″=0.9 kpc. Preliminary analysis of the *Chandra* observation of 3C 371 was presented by Sambruna et al. (2001a).

2. Observations and Data Analysis

Chandra observed 3C 371 on 21 March 2000. The source was at the nominal aimpoint of the ACIS-S3 chip and the exposure was continuous for $\sim$ 10 ks. We used data reprocessed by the *Chandra* X-ray Center using up-to-date calibration files and standard screening procedures which left a net exposure of 10,120 s on-source.

As we were originally interested in the large-scale X-ray environment of the source, no precaution was taken to mitigate pileup of the central core using a subarray mode. Thus, the bright central core is severely piled-up, preventing us from performing any meaningful spectral and detailed spatial analysis of the nucleus. An image was produced by smoothing the raw *Chandra* image with a Gaussian of width=0.3″ in the energy range 0.4–8 keV, where the background is negligible, with final resolution of 0.86″ FWHM. An elongation of the emission in the S-W direction shows up clearly both in the raw and smoothed images. While we can not exclude some contamination from the PSF wings in the innermost ($\lesssim 2''$) parts of the jet, we note that the X-ray jet extends up to $\sim 4''$. More importantly, the X-ray elongation lies at the same position angle as the known radio-optical jet in 3C 371 (Figure 1), which is convincing evidence of its reality.

We also present a new *MERLIN* image of 3C 371, calibrated from unpublished archival data obtained on 1-2 April 1998 as an HI absorption experiment (P.I., A. Pedlar). The target was observed continuously for 18 hours, interleaved with 80-second scans of the nearby phase calibrator 1823+689 every ten minutes. Some editing and the initial data calibration were performed at Jodrell Bank which yielded a single continuum data set at a center frequency of 1.353 GHz with 7.5 MHz total bandwidth. The absolute flux density

[2] Based on observations made with the NASA/ESA *Hubble Space Telescope*, obtained at the Space Telescope Science Institute, which is operated by the Association of Universities for Research in Astronomy, Inc., under NASA contract NAS5–26555.

was brought to the Baars et al. (1977) scale with a single 25-minute scan of 3C 286 set to 15.085 Jy. Phase and gain solutions were then applied to 3C 371 using a point source model for 1823+689. The data were edited and self-calibrated using the Caltech `DIFMAP` package (Shepherd et al. 1994). Appropriate weights were applied to each antenna in order to account for their differing sensitivities. We reached a dynamic range (peak to off-source RMS) of about 6000:1 in the final image (Figure 1) which is not shown at full resolution in order to compare directly with the *Chandra* image. Previous 1.7 GHz MERLIN maps shown at full resolution (Browne & Orr 1981; Akujor et al. 1994) do not clearly show knot B, but we clearly detect this feature in our new image.

Our *HST* WFPC2 F555W image was gaussian smoothed (σ $\sim$0.21″) to mirror the *Chandra* resolution and was presented at full resolution by Scarpa et al. (1999) to which we refer the reader for details on the calibration. The F555W filter closely matches the standard Johnson V-band. Here, we re-extracted fluxes for knots A and B using apertures of radius 0.75″ centered on the knot positions, for consistency with the *Chandra* extraction.

3. Results

Figure 1 shows the 0.4–8 keV ACIS image of 3C 371 (top). Also shown for comparison on the same scale are the images of the jet in the optical (middle) and radio (bottom), from our *HST* and *MERLIN* data. The X-ray jet is clearly apparent in the S-W direction, with the same position angle on the sky as the optical and radio jets. A bright X-ray structure is visible at $\sim 1.7''$ from the core, after which the X-ray suface brightness decreases with fainter X-ray emission present up to $\sim 4''$. A total of 360 counts are collected from the X-ray jet in 0.4–8 keV, of which $\sim$ 260 are in the first feature. Due to the limited statistics, it is difficult to determine whether the first bright "knot" is resolved or not.

Comparing the multiwavelength morphologies of the jet, the brighter structure in the X-ray jet appears to coincide with optical knot B (following the nomenclature of Scarpa et al. 1999). At this position both the radio and optical jets show relatively fainter emission spots. If the X-ray feature is real, this indicates a large difference of the X-ray morphology with respect to the optical and radio one. Our optimally designed *Chandra* GO3 observations will better define the jet X-ray morphology close to the nucleus.

We extracted the X-ray spectrum of knot B using a circular region of radius 0.75″. To correct for contamination due to the core PSF, we extracted spectra from a region with the same radius and at the same distance from the core (1.8″), but at different azimuth positions, to check for any systematic effects. We then subtracted these spectra from the X-ray spectrum of knot B, and performed spectral fits on the subtracted data. We find that the spectral fit results do not depend on the azimuth position. After subtraction, the spectrum of knot B contains 229 counts in 0.2–8 keV, and is consistent with a power law, absorbed by Galactic N_H only (4.9×10^{20} cm^{-2}). The column density was fixed to Galactic during the fits. The fitted photon index is $\Gamma = 1.7$ in the range (1.5, 2.1) at 90% confidence level. The 2–10 keV flux is $F_{2-10\ keV} \sim 1 \times 10^{-13}$ erg cm^{-2} s^{-1}. The fit is good, with χ^2=6 for 9 degrees of freedom.

For the remaining, fainter part of X-ray jet, we measure $\sim$ 100 counts. Assuming a power-law spectrum with $\Gamma = 2$ and Galactic N_H, the 2–10 keV flux is 2.6×10^{-14} erg cm^{-2} s^{-1}. This region coincides with knot A in the optical and radio images (Scarpa et al. 1999).

4. Discussion and Conclusions

Using a short (10 ks) *Chandra* image we have detected the X-ray counterpart of the radio-optical jet in the nearby radio galaxy 3C 371. Comparison with the optical and radio morphology from a reanalysis of archival *HST* and *MERLIN* data shows that the peak X-ray emission from the jet does not coincide with the brightest knot at longer wavelengths. Future deeper *Chandra* images are needed to confirm this result.

Figure 2 shows the Spectral Energy Distributions (SEDs) from radio to X-rays of knots B and A. For the *MERLIN* image, we summed the clean components within the specified apertures within the (u,v) plane rather than the image plane. In both knots, the fluxes at all three wavelengths were extracted in the same circular region with radius 0.75″. Figure 2 shows that in both cases

the X-ray flux is below the extrapolation from the radio-to-optical continuum. The latter is slightly steeper for knot A than for knot B.

While the radio to optical continuum is due to synchrotron radiation, the radiative mechanisms usually considered as the possible origin of X-rays are either synchrotron or inverse Compton (IC) scattering on various possible sources of soft photons (Celotti, Ghisellini, & Chiaberge 2001). An analysis similar to PKS 0637–752 (Tavecchio et al. 2000) indicates that IC emission either on the internal synchrotron photons (SSC) or on the Cosmic Microwave Background (CMB) photons can not explain the SED of knot B, unless the source is characterized by an extremely high Doppler factor ($\delta \sim 50$) or is very far from equipartition (Figure 3).

The most natural interpretation of the SEDs is that the X-rays are due to synchrotron emission from the same population of relativistic electrons responsible for the longer wavelengths. In this scenario the steepening of the optical-to-X-ray continuum between knots B and A can be attributed to synchrotron radiative losses. A steep X-ray spectrum is predicted by this scenario ($\Gamma > 2$) for knot B, consistent with the fitted value of the photonx index within the 90% uncertainties (see above).

Applying a synchrotron homogeneous model, and assuming equipartition, we derive a magnetic field of few 10^{-5} G and a Doppler factor of a few (for a knot radius of $\sim 10^{21}$ cm, or $1''$), consistent with the jet-to-counterjet ratio from the radio (§ 1). The derived electron lifetimes at 1 keV (electrons with Lorentz factor $\gamma \simeq 3 \times 10^7$) are short enough ($\sim 10^{10}$ s) for the electrons to effectively cool in the knot (Fig. 4). The different X-ray morphology could be related, in this picture, to the short cooling time of X-ray emitting electrons. Electrons producing X-rays cool rapidly after knot B, while optical and radio electrons can survive until they reach the bright knot A at $\sim 3''$, where emission can be enhanced by compression, by a larger magnetic field and/or by repeated acceleration with lower maximum energy.

It is instructive to compare 3C 371 with two other well studied sources with X-ray jets, namely PKS 0637–752 and 3C 273. In the former, the radio, optical and X-ray morphologies are quite similar (Chartas et al. 2000; Schwartz et al. 2000) and it is possible to explain quite well the X-ray emission as due to IC/CMB scattering off the jet electrons (Tavecchio et al. 2000). For 3C 273 the situation is more complex, with the global radio and X-ray morphology being anticorrelated along the jet (Sambruna et al. 2001b). We proposed that the dominant X-ray emission mechanism is IC from CMB, although the evidence is not conclusive (see Marshall et al. 2001 for a different interpretation). It is tempting to speculate that 3C 371 and PKS 0637–752 represent the prototypes of "pure" synchrotron and IC/CMB sources, respectively, while 3C 273 is an intermediate case, where both processes contribute to the total X-ray flux. Clearly, a larger sample of sources with different morphologies and SEDs is necessary to discuss the importance of the two mechanisms in different sources, which we anticipate from our ongoing *Chandra*/*HST* GO2 survey of radio jets.

In conclusion, a new X-ray jet has been detected in 3C 371 in a short *Chandra* exposure. Despite the limited signal-to-noise ratio of the X-ray data, an intriguing morphology is apparent, with most of the X-ray counts coming from a region of relative minimum radio and optical emission. The broad-band SED at two different locations in the jet are consistent with a synchrotron origin for the X-rays. Deeper *Chandra* and *HST* observations of 3C 371 are planned, which will allow us to confirm the X-ray morphology of the jet and measure accurately its spectrum as a function of position along the jet.

We thank the referee, George Chartas, for helpful comments. We also thank Anita Richards for helpful discussions and for performing the initial calibration of the archive *MERLIN* data, Alan Pedlar for permission to use this data, and Dan Homan for the `PGPLOT` script used to produce Figure 1. Support for this work was provided by NASA grants NAS8–39073 (JEP), NAG5–10073 (RMS), and through grant NAG5–9327, and grant GO-06363.01-95A from the Space Telescope Science Institute, which is operated by AURA, Inc., under NASA contract NAS 5-26555 (CMU, RS, CCC). FT and LM aknowledge partial financial support from the Italian MURST-COFIN-2000, from ASI-R-105-00 and from the European Commission ERBFMRX-CT98-0195. *MERLIN* is a UK National Facility operated by the University

of Manchester at Jodrell Bank Observatory on behalf of PPARC.

REFERENCES

Akujor, C.E., Lüdke, E., Browne, I.W.A., Leahy, J.P., Garrington, S.T., Jackson, N., & Thomasson, P. 1994, A&AS, 105, 247

Baars, J.W.M., Genzel, R., Pauliny-Toth, I.I.K., & Witzel, A. 1977, A&A, 61, 99

Biretta, J.A. et al. 1991, AJ, 101, 1632

Bridle, A.H. & Perley, R.A. 1984, ARA&A, 22, 319

Browne, I.W.A. & Orr, M.J.L. 1981, Proc. of the Second ESO/ESA Workshop "Optical Jets in Galaxies", ESA SP-162 (Paris: European Space Agency), p. 87

Celotti, A., Ghisellini, G., & Chiaberge, M. 2001, MNRAS, 321, L1

Chartas, G. et al. 2000, ApJ, 542, 655

Feigelson, E.D. et al. 1981, ApJ, 251, 31

Gomez, J.-L. & Marscher, A.P. 2000, ApJ, 530, 245

Harris, D.E. & Stern, C.P. 1987, ApJ, 313, 136

Marshall, H.L. et al. 2001, ApJ, 549, L167

Miller, J.S. 1975, ApJ, 200, L55

Nilsson, K. et al. 1997, ApJ, 484, L107

Sambruna, R.M. et al. 2001a, Proc. of the Workshop "Blazar Physics and Demographics", held at STScI, Baltimore, MD, 2000 July 12–14, ed. P.Padovani and C.M.Urry, PASP, in press

Sambruna, R.M. et al. 2001b, ApJ, 549, L161

Scarpa, R., Urry, C.M., Falomo, R., & Treves, A. 1999, ApJ, 526, 643

Schwartz, D.A. et al. 2000, ApJ, 540, L69

Shepherd, M.C., Pearson, T.J., & Taylor, G.B. 1994, BAAS, 26, 987

Sparks, W.B., Biretta, J.A., & Macchetto, F. 1994, ApJS, 90, 909

Tavecchio, F., Maraschi, L., Sambruna, R.M., & Urry, C.M. 2000, ApJ, 544, L23

Wilson, A.S., Young, A.J., & Shopbell, P.L. 2001, ApJ, 547, 740

Wrobel, J.M. & Lind, K.R. 1990, ApJ, 348, 135

This 2-column preprint was prepared with the AAS LaTeX macros v5.0.

See color image: fig1.gif

Fig. 1.— Multiwavelength images of the jet of 3C 371. From top to bottom: *Chandra* ACIS-S (0.4–8 keV), *HST* WFPC2 F555W, and *MERLIN* 1.4 GHz. North is up and East is to the left. The colors are shown logarithmically; the core and inner jet in the radio and optical images were saturated in order to show more detail in the jet. The X-ray image was smoothed with a Gaussian of width 0.3″, achieving final resolution of 0.86″ FWHM. In order to show the inner knot B, the optical image was smoothed with a Gaussian of width 0.21″, achieving final resolution 0.5″ FWHM. The radio image was restored with a beam of 0.5″ FWHM. The feature NE of the optical core is an artifact due to subtraction of the diffraction spikes.

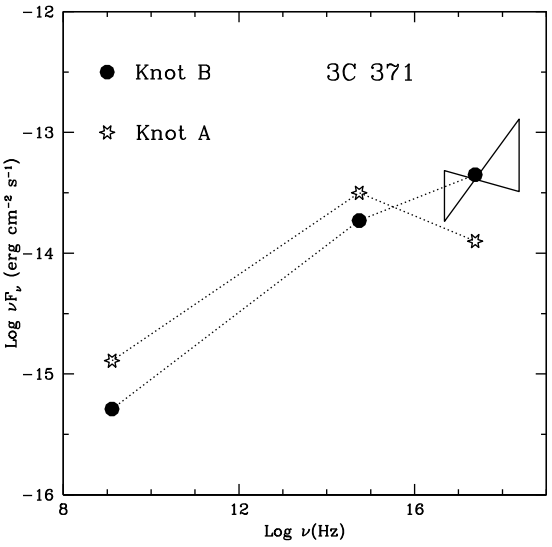

Fig. 2.— Spectral Energy Distributions (SEDs) of two knots of the 3C 371 jet (see Figure 1 and § 4). In both cases, the X-ray flux lies under the extrapolation of the radio-to-optical continuum. A synchrotron model best accounts for both SEDs (see text), yielding B=1.6×10^{-5} G, $\delta = 6$, $\gamma_{max} = 4 \times 10^7$.

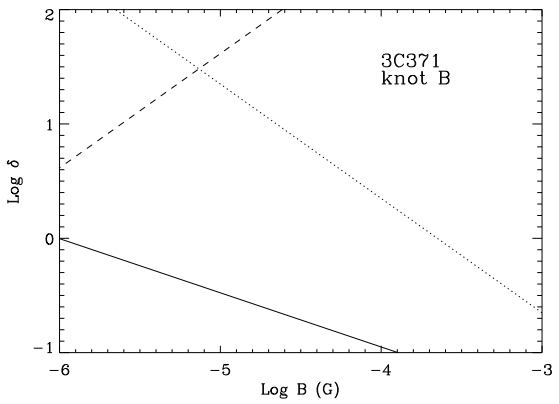

Fig. 3.— Allowed values of the the magnetic field B and the Doppler factor δ for knot B of 3C 371. *Solid line:* Allowed values of B, δ if the X-ray emission is due to SSC. *Dashed line:* Allowed values of B, δ if the X-ray emission is due to CMB. *Dotted line:* Allowed values under the assumption of equipartition between the radiating particles and the magnetic field. Neither SSC or CMB can account for the X-ray emission from knot B, unless the source is characterized by an extremely high Doppler factor ($\delta \sim 50$) or is very far from equipartition.

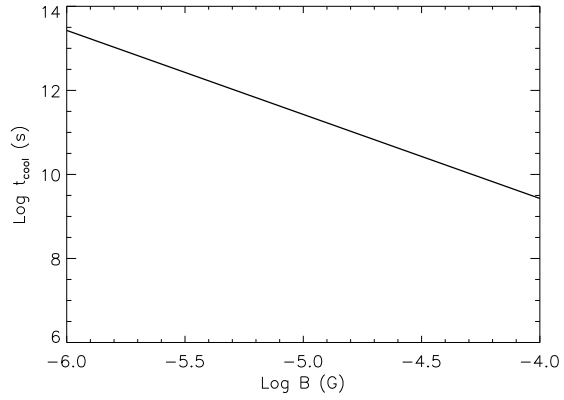

Fig. 4.— Synchrotron cooling time for electrons producing 1 keV photons for different values of the magnetic field and assuming equipartition. For $B \simeq 3 \times 10^{-5}$ G the estimated cooling time is $\sim 10^{10}$ s (see text).